ACS OMEGA

http://pubs.acs.org/journal/acsodf

Article

Experimental and Modeling Investigation on the Pyrolysis of *n*-Decane Initiated by Nitropropane. Part I: 1-Nitropropane

Zhenjian Jia, Jiuzhong Yang, Weixing Zhou,* and Kaiping Yu

Cite This: *ACS Omega* 2023, 8, 15384−15396

Read Online

ACCESS | Metrics & More | Article Recommendations | Supporting Information

ABSTRACT: Initiators can accelerate the pyrolysis of hydrocarbon fuels, thereby reducing the required reaction temperature in the hypersonic vehicle heat exchanger/reactor. Nitro-alkanes are considered as efficient initiators due to their lower energy barrier of the C−N bond cleavage reaction. To research the mechanism of the initiation effect of nitro-alkanes on the decomposition of hydrocarbon fuel, synchrotron radiation vacuum ultraviolet photoionization-mass spectrometry (SVUV-PIMS) was employed to experimentally study the pyrolysis of *n*-$C_{10}H_{22}$, 1-$C_3H_7NO_2$, and their binary mixtures in a flow tube under pressures of 30 and 760 Torr. The species identified and measured in the experiments included alkanes, alkenes, dialkenes, alkynes, nitrogen oxides, benzene, and free radicals, which revealed the mechanism of *n*-decane and 1-$C_3H_7NO_2$ pyrolysis, as well as the interactions of the two fuels. Experiments show that the presence of 1-$C_3H_7NO_2$ reduces the initial decomposition temperature of *n*-$C_{10}H_{22}$, and the increased pressures could achieve a stronger promoting effect on the conversion of *n*-$C_{10}H_{22}$. A detailed kinetic model containing 1769 reactions and 278 species was established and validated based on the mole fraction distributions of *n*-$C_{10}H_{22}$, major pyrolysis species, and important intermediates measured in pure fuel and initiated pyrolysis. The kinetic model can accurately predict the experimental data, and the mechanism of 1-$C_3H_7NO_2$-initiated pyrolysis of *n*-$C_{10}H_{22}$ is analyzed with the model. The effect of 1-$C_3H_7NO_2$ on the consumption of *n*-$C_{10}H_{22}$ and selectivity of cracked products is highlighted.

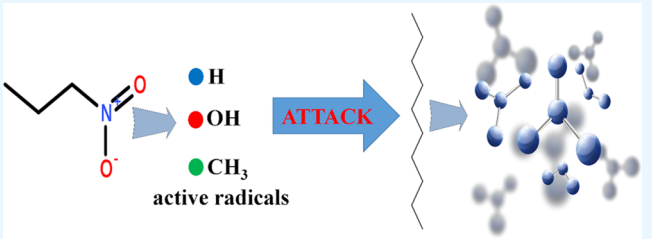

1. INTRODUCTION

With the continuous development of advanced aeroengines for supersonic aircraft, the thermal protection problems caused by high-intensity combustion in the engine and the friction between the engine and the air at high flight speeds urgently need to be solved.[1,2] Endothermic hydrocarbons have been proven to be an effective solution to the thermal protection problem of the engine.[3−6] Compared with traditional fuels, their endothermic capabilities are limited by their physical heat sinks. Endothermic hydrocarbon fuels will undergo pyrolysis and endothermic reactions at a specific temperature. The extra heat sink brought by the endothermic reaction significantly improves the heat-absorption and heat-transfer capacity of the fuel, making it a substitute for traditional fuels.[6,7] Since the physical, sensible heat of conventional fuel is already determined by its composition, improving the chemical heat sink of the fuel is crucial to improve the heat-absorption capacity of endothermic hydrocarbon fuels.

A high reaction temperature is needed to achieve a conversion that meets the heat-sink requirements in the hydrocarbon fuel thermal pyrolysis process. High temperatures will increase the material's allowable temperature requirements, reduce the material's performance, and cause a large amount of coking and carbon deposition to affect flow of heat transfer or cause pipeline blockage.[8,9] The thermal pyrolysis of hydrocarbon fuel is a typical chain reaction process, and the generation of active radicals from fuel pyrolysis is the committed step in determining the speed of fuel decomposition. However, the bond energy of C−H or C−C bonds in fuel molecules is relatively high. It is difficult for C−C and C−H bonds to break at lower temperatures (usually, the fuel starts to crack when the temperature reaches above 500 °C), which is a reaction step that restricts fuel pyrolysis in the course of the cleavage chain reaction.[10] Therefore, adding a small amount of initiator into the hydrocarbon fuel can produce a large number of active free radicals that can react with the fuel at a lower temperature, reduce the initial pyrolysis temperature of the fuel, and promote the pyrolysis of the fuel so that the fuel can reach the required pyrolysis rate for thermal protection at a lower temperature.[11]

In recent years, plenty of research has been carried out on the initiated pyrolysis of hydrocarbon fuels. Some studies have used experimental methods to analyze the effects of initiators on fuel decomposition[11−19] and heat-sink characteristics.[20,21]

Received: February 1, 2023
Accepted: April 12, 2023
Published: April 20, 2023

https://doi.org/10.1021/acsomega.3c00508
ACS Omega 2023, 8, 15384−15396

Chang et al.[12−14] found that adding sulfur dioxide, hydrogen peroxide, acetone, di-*tert*-butyl phenol, or nitromethane to fuel can effectively reduce the pyrolysis temperature and enhance pyrolysis. Meanwhile, the results indicated that the effect of the initiator is related to the properties of the initiator and the fuel. Wickham et al.[11] investigated the promoting effect of the initiator on *n*-C_7H_{16} pyrolysis under supercritical conditions. The experimental results showed that an initiator content of only 2% mass fraction increased the fuel pyrolysis rate twice. The effect of initiators on the heat sinks of cyclohexane, Norpar-12, JP-7, and *n*-$C_{10}H_{22}$ was subsequently studied,[20,21] and it was found that the heat sinks for these four fuels were improved. Others compared the effects of different initiators and screened the best initiators.[22−24] Chakraborty et al.[24] studied the effects of di-*tert*-butyl peroxide, di-isopropyl-amine, and triethylamine on n-heptane through a flow reactor. They found that all initiators could promote *n*-C_7H_{16} pyrolysis, and the results indicated that the initiator triethylamine had the best promotion effect. The promotion effect of 1-$C_3H_7NO_2$ (1-NP), triethylamine (TEA), and 3,6,9-triethyl-3,6,9-trimethyl-1,4,7-triperoxynonane (TEMPO) on the pyrolysis of *n*-$C_{12}H_{26}$ was investigated by Liu et al.[22,23] The experimental results showed that the promotion order was NP > TEMPO > TEA. All of the above research shows that the selected initiators could promote the pyrolysis of the hydrocarbon fuel and increase the heat sink at lower temperatures. In addition, some studies also compared the promotion effect of different initiators on fuel pyrolysis by experimental methods[22−24] and reactive molecular dynamics (MD) simulation methods.[25] In terms of the impact on fuel pyrolysis products, Wickham et al.[11] found that the product distribution was less affected by adding an initiator under supercritical pressure. Chakraborty et al.[24] found that the added initiator had an effect when the fuel pyrolysis rate was low, and its effect was negligible when the fuel pyrolysis rate was high. Guan et al.[26,27] studied the initial pyrolysis path of *n*-alkane/nitro-alkane-initiated pyrolysis by the quantum chemical calculation method and obtained four possible initial reactions according to the calculation results of activation energy.

In summary, the previous research on initiated pyrolysis focuses on macroscopic aspects such as improving the fuel pyrolysis rate and heat sink. There are few kinetic studies to reveal the action mechanism of initiators. The critical problem is detecting various intermediates and products in real time and in situ for a specific and comprehensive understanding of the kinetic mechanism in the initiated pyrolysis. SVUV-PIMS technology, due to its wide tunability of energy and excellent energy resolution, can minimize vacuum ultraviolet photoionization fragment interference and distinguish isomers and detect active free radicals. At present, SVUV-PIMS technology has been successfully applied in combustion diagnosis. Combustion species, especially free radicals and intermediates have been analyzed and detected, and reliable experimental data have been provided.[28] Considering the advantages of SVUV-PIMS in detecting species, especially free radicals that play a crucial role in initiated pyrolysis, this technology enables real-time detection of both stable species and reactive intermediates.

Additionally, a detailed kinetic model of the reaction describing the initiated pyrolysis process is necessary to reveal the action mechanism of an initiator. In previous studies, we used vacuum ultraviolet photoionization-mass spectrometry technology combined with a flow-tube pyrolysis experimental device to study the initiated pyrolysis of nitromethane/*n*-$C_{10}H_{22}$. A detailed reaction kinetic model was established and used to analyze the effect of the initiator nitromethane on the pyrolysis of *n*-$C_{10}H_{22}$.[29]

This work aims to study the pyrolysis of *n*-$C_{10}H_{22}$ and 1-$C_3H_7NO_2$ in a flow-tube reactor combined with SVUV-PIMS technology and explore the kinetic mechanism of *n*-$C_{10}H_{22}$ pyrolysis initiated by 1-$C_3H_7NO_2$ at different temperatures and pressures. *n*-$C_{10}H_{22}$ was selected as fuel based on the following two aspects. First, *n*-$C_{10}H_{22}$ is one of the main components of aviation propulsion fuel. As a typical component of long-chain *n*-alkane, it is often used as a propellant fuel or aviation kerosene surrogate component to study the actual fuel performance. On the other hand, much experimental and theoretical research has been carried out on the combustion and pyrolysis of *n*-$C_{10}H_{22}$,[30−37] and their respective reaction kinetic models have been developed. Many kinetic models have been verified by experiments and have good simulation accuracy.[31,32] Meanwhile, experiments and theoretical calculations indicate that 1-$C_3H_7NO_2$ can reduce the actual cracking temperature of hydrocarbon fuel and improve the fuel cracking rate. 1-$C_3H_7NO_2$ has been confirmed to have good initiating properties,[23,25] and it will be used as an initiator in the experiments.

In this work, stable species and intermediates, especially free radicals, were detected in the experiment. The detailed reaction kinetic model of *n*-$C_{10}H_{22}$/1-$C_3H_7NO_2$ pyrolysis was established based on the experiment, and the results verified the accuracy of the kinetic model under different experimental conditions. Finally, the reaction process of *n*-$C_{10}H_{22}$ pyrolysis initiated by 1-$C_3H_7NO_2$ was analyzed by the model, the initiation and acceleration effect of the initiator on fuel pyrolysis and the influence on the distribution of pyrolysis products were deeply understood, and the initiation mechanism of 1-$C_3H_7NO_2$ on *n*-$C_{10}H_{22}$ was obtained.

2. EXPERIMENTAL METHODS

The experiments in this work were carried out at the Combustion and Flame Beamline Station (BL03U) of the National Synchrotron Radiation Laboratory (NSRL), University of Science and Technology of China. The experimental setup is similar to the pyrolysis of nitromethane (NM) and nitroethane (NE)[38,39] at NSRL. A detailed description can be found in the literature,[28,40−46] so a detailed introduction will not be given here. The experimental device is a flow-tube reactor combined with a synchrotron radiation photoionization-mass spectrometer, including four parts: pyrolysis furnace, differential pumping chamber, photoionization chamber, and reflectron time-of-flight mass spectrometer. The fuel diluted by argon (Ar) was pumped into an alumina flow reactor with a length of 22 cm and an inner diameter of 0.68 cm. The reactor is fixed in the pyrolysis chamber and heated by electric heating wires evenly wrapped around the outside. The pressure in the reactor was controlled by the MKS throttle valve and measured by the MKS capacitive pressure gauge. The temperature distribution in the reactor was measured by a thermocouple near the middle of the reaction zone.[28,40−46] The temperature measurement and pressure calculation methods can be found in the literature,[40] and the temperature file is provided in Tables S1 and S2. The pressure along the tube can be considered constant in this work because the pressure drop along the reactor was very small at pressures above 30 Torr.[47] The fuel and Ar flow rates were controlled by two mass flow

https://doi.org/10.1021/acsomega.3c00508
ACS Omega 2023, 8, 15384−15396

controllers (MKS). The detailed experimental conditions are shown in Table 1.

Table 1. Experimental Conditions

pressure, Torr	temperature, K	flow rate of Ar, sccm	fuel	flow rate of fuel, sccm
30, 760	700−1400	990	n-$C_{10}H_{22}$	10
			1-$C_3H_7NO_2$	10
		980	n-$C_{10}H_{22}$	10
			1-$C_3H_7NO_2$	10

The pyrolysis components, including stable species and intermediates, were sampled through a quartz nozzle fixed ∼1 cm downstream of the flow reactor outlet, followed by molecular beam formation. After ionizing the molecular beam under VUV light, the reflection time-of-flight mass spectrometer detected ion signals of various species with a resolution of up to 3000 Å. Species were determined by comparing ionization energies (IEs) measured from near-threshold photoionization efficiency (PIE) spectra with values in the literature, and the molar fractions of the components were determined from near-threshold photoionization efficiency spectra measured at different temperatures (PIEs). Component identification and molar fraction calculations are described in detail in the literature.[44,48] The molar fraction uncertainty of the major species is ±5−10%, the mole fraction of intermediates with known photoionization cross sections (PICs) is ∼±25%, and the molar fraction uncertainty of the species using estimated PICS is ∼2.

3. KINETIC MODEL

The detailed kinetic model in this work was established based on our previous study on the initiated pyrolysis of n-$C_{10}H_{22}$ using nitromethane as an initiator.[29] The $C_2H_5NO_2$ pyrolysis mechanism[39] was added to the model. The submechanism of 1-$C_3H_7NO_2$ has been updated according to the latest experimental and theoretical calculation results.[49−51] Table 2 lists part of the submechanisms of 1-$C_3H_7NO_2$ and its derived radicals. The n-$C_{10}H_{22}$/1-$C_3H_7NO_2$ reaction mechanism includes 1769 reactions and 278 species. There is less literature on the elementary reaction of 1-$C_3H_7NO_2$; therefore, for other reactions in the submechanism of 1-$C_3H_7NO_2$, the rate constants must be determined by analogy with the reactions of other species, i.e., C_3H_8,[5252] $C_2H_5NO_2$,[39] and propanol.[53]

4. RESULTS AND DISCUSSION

4.1. Pyrolysis of 1-$C_3H_7NO_2$. Figures 1 and 2 show the experimental and simulated mole fraction of species in 1-$C_3H_7NO_2$ pyrolysis under different pressures. The kinetic model we developed reproduces the experimentally measured mole fraction distributions of products well. Under 30 and 760 Torr pressures, the decomposition of 1-$C_3H_7NO_2$ starts at ∼821 and 722 K, respectively. At 1062 and 846 K, 1-$C_3H_7NO_2$

Table 2. 1-$C_3H_7NO_2$ Reaction Subset

reaction	A (s^{-1})	n	E_a (cal mol^{-1})	source
$C_3H_7NO_2 = C_3H_7 + NO_2$	3.568×10^{20}	−1.539	62 532.2	49
PLOG/0.0001	1.557×10^{72}	−18.386	77 252.9	
PLOG/0.001	1.500×10^{83}	−21.059	86 738.1	
PLOG/0.01	3.361×10^{83}	−17.063	80 641.9	
PLOG/0.1	5.668×10^{59}	−13.691	75 228.3	
PLOG/1	3.627×10^{71}	−16.548	89 986.4	
PLOG/10	2.087×10^{65}	−14.446	90 192.2	
PLOG/100	3.617×10^{64}	−13.866	96 322.5	
$C_3H_7NO_2 = C_3H_6 + HONO$	2.641×10^{8}	1.338	47 406.5	49
PLOG/0.0001	1.068×10^{71}	−18.098	70 905.2	
PLOG/0.001	1.075×10^{78}	−19.750	78 566.8	
PLOG/0.01	1.607×10^{66}	−16.081	73 464.8	
PLOG/0.1	7.642×10^{55}	−13.691	75 228.3	
PLOG/1	2.598×10^{64}	−14.912	80 659.0	
PLOG/10	3.592×10^{57}	−12.683	80 246.7	
PLOG/100	3.406×10^{53}	−11.250	82 975.1	
$C_3H_7NO_2 = C_2H_4 + HCNO + H_2O$	7.240×10^{7}	1.42	26 990.6	51
$C_3H_7NO_2 = CH_3CH_2CH_2ONO$	3.430×10^{11}	0.82	30 924.1	51
$C_3H_7NO_2 + H = CH_2CH_2CH_2NO_2 + H_2$	1.300×10^{6}	2.54	6756	$k_{C_3H_8+H}$
$C_3H_7NO_2 + H = CH_3CHCH_2NO_2 + H_2$	1.300×10^{6}	2.40	4471	$k_{C_3H_8+H}$
$C_3H_7NO_2 + H = CH_3CH_2CHNO_2 + H_2$	6.470×10^{13}	−0.33	5380	$k_{C_3H_8OH+H}$
$C_3H_7NO_2 + H = C_3H_7NO + OH$	1.400×10^{12}	0.00	3730	$k_{CH_3NO_2+H}$
$CH_3CH_2CH_2O + NO = CH_3CH_2CH_2ONO$	1.200×10^{13}	0.00	−143	$k_{CH_3CH_2ONO}$
$CH_2CH_2CH_2NO_2 = C_3H_6 + NO_2$	2.000×10^{12}	0.00	0.00	$k_{C_3H_7\rightarrow C_3H_6}$
$CH_3CHCH_2NO_2 = C_3H_6 + NO_2$	5.700×10^{9}	1.16	874	$k_{iC_3H_7\rightarrow C_3H_6}$
$CH_3CH_2CHNO_2 = C_3H_6 + NO_2$	2.000×10^{12}	0.00	0.00	$k_{C_3H_7\rightarrow C_3H_6}$
$C_3H_7NO + H = C_3H_6 + NO + H_2$	1.300×10^{6}	2.54	6756	$k_{C_3H_8+H}$
$C_3H_7NO + H = CH_3CH_2CHNO + H_2$	4.400×10^{8}	1.5	378	k_{CH_3NO+H}
$CH_3CH_2CHNO = C_3H_6 + NO$	2.000×10^{12}	0.00	0.00	$k_{C_3H_7\rightarrow C_3H_6}$

https://doi.org/10.1021/acsomega.3c00508
ACS Omega 2023, 8, 15384−15396

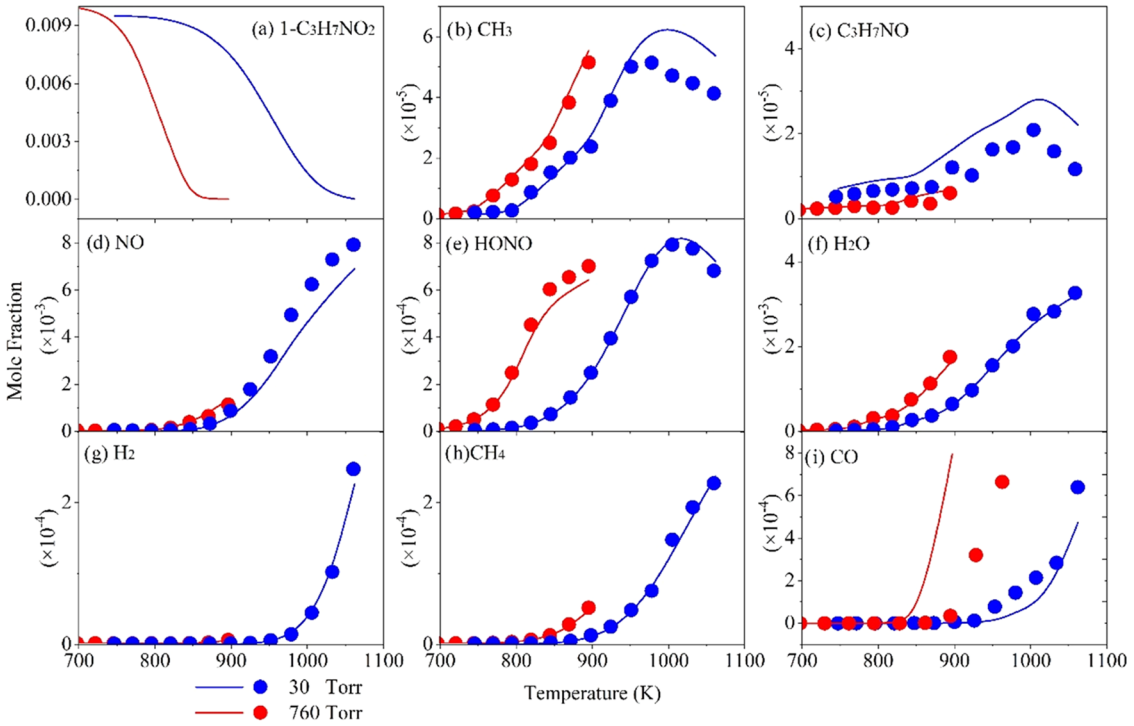

Figure 1. Simulated (solid lines) and experimental (symbols) mole fractions of (a) 1-$C_3H_7NO_2$, (b) CH_3, (c) C_3H_7NO, (d) NO, (e) HONO, (f) H_2O, (g) H_2, (h) CH_4, and (i) CO in 1-$C_3H_7NO_2$ pyrolysis at 30 and 760 Torr.

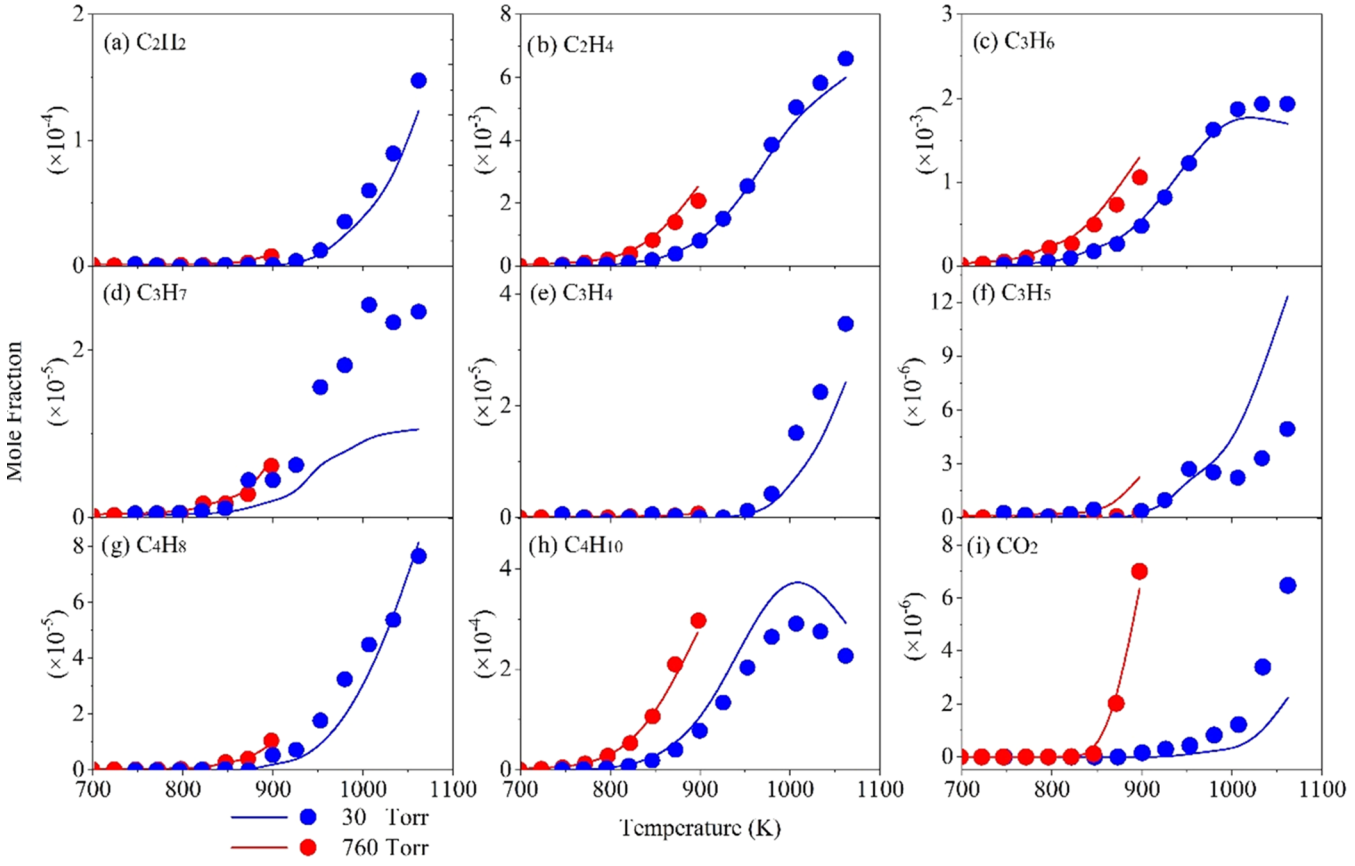

Figure 2. Simulated (solid lines) and experimental (symbols) mole fractions of (a) C_2H_2, (b) C_2H_4, (c) C_3H_6, (d) C_3H_7, (e) C_3H_4, (f) C_3H_5, (g) C_4H_8, (h) C_4H_{10}, and (i) CO_2 in 1-$C_3H_7NO_2$ pyrolysis at 30 and 760 Torr.

is almost entirely consumed, as shown in Figure 1a. It can be seen from Figure 2 that C_2H_4 and C_3H_6 are the most abundant hydrocarbons, which can be generated from the decomposition of C_3H_7 radicals formed by C−N bond cleavage. It can also be

https://doi.org/10.1021/acsomega.3c00508
ACS Omega 2023, 8, 15384−15396

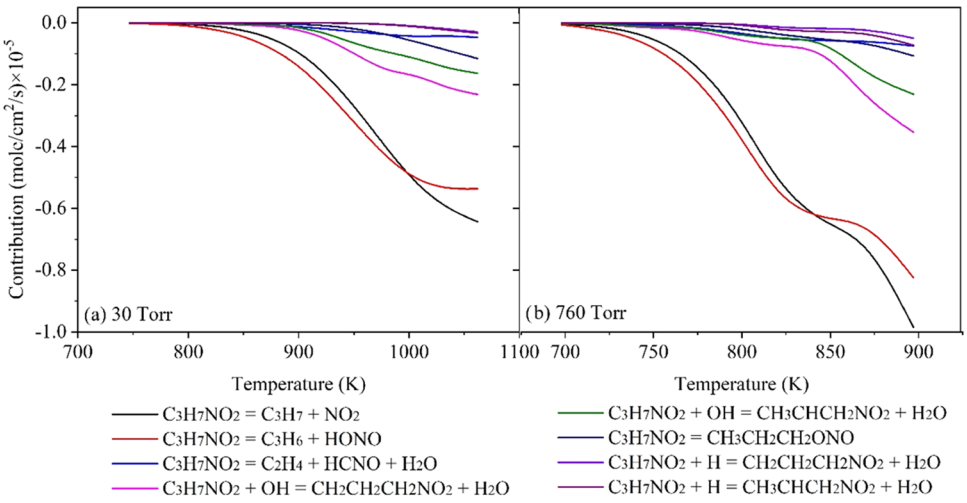

Figure 3. ROP analysis of 1-$C_3H_7NO_2$ along with the reactor distance.

generated from 1-$C_3H_7NO_2$ by a concerted molecular elimination (CME) mechanism.[49,51] Figure 1d shows that NO is the most abundant in the NO_x component, with a comparable concentration to that of C_2H_4 due to the high reactivity of NO_2 as an oxidant.[39] NO_2 is reduced to NO by oxidizing hydrocarbon radicals generated during 1-$C_3H_7NO_2$ pyrolysis. In the present study, no oxidant was provided in the initial reactants. The oxidation process of the components relies on the secondary reaction between the hydrocarbon components and NOx, which is insufficient for complete oxidization.

CH_4, H_2O, H_2, CO, and CO_2 were considered to be the final products whose mole fractions are shown in Figures 1f–i and 2i. The simulated mole fraction distributions of H_2O, H_2, and CH_4 are in good agreement with the experimental results. For CO and CO_2, there are some deviations between the experimental and simulation results. This is probably because the rate constants of some significant reactions have no pressure dependence in the 1-$C_3H_7NO_2$ mechanism in this work. For example, reactions $CH_3CH_2CHNO = C_3H_6 + NO$ and $nC_3H7 + NO = C_3H_7NO$, but the overall agreement is satisfactory. Hydrocarbon radicals have been identified in the experiments. Figures 1b and 2d show the mole fraction distribution of methyl and propyl radicals. The detection results of propyl and NO_2 support the occurrence of the 1-$C_3H_7NO_2$ C–N bond cleavage reaction. C_3H_7 can generate C_2H_4 and methyl groups through a β-C–C scission reaction. The deviation between the simulation and experimental results for the radical mole fraction is attributed to the experimental error caused by the uncertainty of the photoionization cross section free radical. Other less concentrated species, C_2H_2, C_3H_4, C_4H_8, and C_4H_{10} were also detected in the experiment, as shown in Figure 2.

To investigate the reaction pathway for the pyrolysis of 1-$C_3H_7NO_2$ under the experimental conditions in this work, a rate of production analysis (ROP) was carried out. For comparison purposes, the contribution of different reactions to 1-$C_3H_7NO_2$ consumption at each temperature condition was integrated over the reactor flow direction. Eight reactions with the largest contribution to fuel consumption were considered in the analysis, and the contributions of these reactions along with temperature are shown in Figure 3. The results show that the main pathways for the decomposition of 1-$C_3H_7NO_2$ are the C–N bond cleavage reaction and the CME pathway due to the lower reaction energy barrier of the reactions.[49,51] At the same time, Figure 3 shows that the two reactions that dominate the consumption of 1-$C_3H_7NO_2$ have roughly equal contributions within a specific range. With increasing temperature, the contribution of the C–N bond cleavage reaction will be higher than that of the CME reaction, and this phenomenon is similar to that of nitroethane pyrolysis.[39] The secondary reaction is dominated by the pyrolysis species generated by the primary decomposition of 1-$C_3H_7NO_2$. At 30 and 760 Torr, the hydrogen abstraction reaction of 1-$C_3H_7NO_2$ starts at ~900 and 746 K, respectively, and these reactions have small contributions to the conversion of 1-$C_3H_7NO_2$. The rate of these reactions is dominated by the formation of OH, which is mainly derived from the secondary reaction $NO_2 + H = NO + OH$. The pyrolysis of 1-$C_3H_7NO_2$ has a CME channel to generate C_3H_6 and HONO. Then, the decomposition of HONO provides a second source of OH radicals that facilitate the abstraction of hydrogen from the fuel. Due to the high energy barrier, the isomerization of 1-$C_3H_7NO_2$ to ethyl nitrite followed by decomposition to propanal and NO is not significant at the current experimental temperature.

To study the pyrolysis process of 1-$C_3H_7NO_2$, the ROP analysis of the main intermediates in the reaction process was carried out. Figure 4 shows the main pyrolysis path diagram for 1-$C_3H_7NO_2$ with a pyrolysis rate of 50% under a pressure of 30 Torr and a temperature of 1062 K. Both the CME and C–N

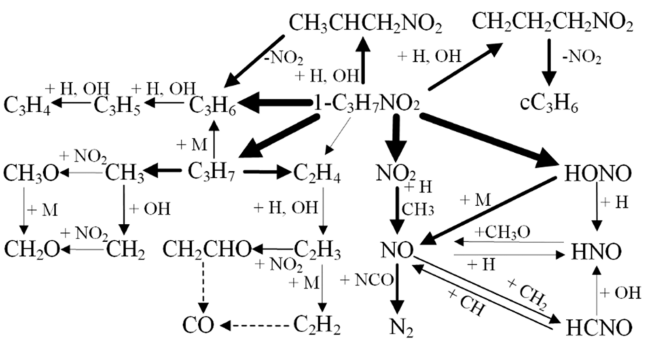

Figure 4. Reactions pathway diagram based on ROP analysis of 1-$C_3H_7NO_2$ pyrolysis under a pressure of 30 Torr.

https://doi.org/10.1021/acsomega.3c00508
ACS Omega 2023, 8, 15384–15396

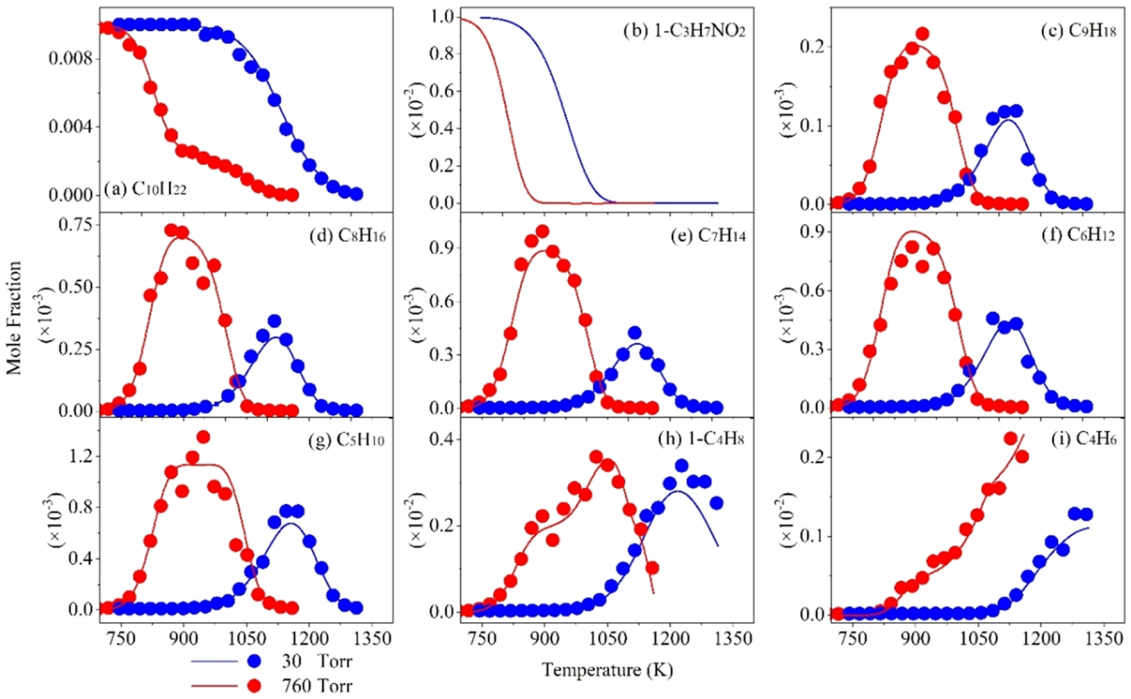

Figure 5. Simulated (solid lines) and experimental (symbols) mole fractions of (a) n-$C_{10}H_{22}$, (b) 1-$C_3H_7NO_2$, (c) C_9H_{18}, (d) C_8H_{16}, (e) C_7H_{14}, (f) C_6H_{12}, (g) C_5H_{10}, (h) C_4H_8, and (i) C_4H_6 in n-$C_{10}H_{22}$/1-$C_3H_7NO_2$ initiated pyrolysis at 30 and 760 Torr.

bond cleavage reaction pathways result in the separation of nitrogen-containing products (NO_2, HONO, and HCNO) from the hydrocarbon products (C_3H_6, C_3H_7, and C_2H_4). It can also be found that $CH_2CH_2CH_2NO_2$, $CH_3CHCH_2NO_2$, and C_3H_7ONO are formed by hydrogen abstraction reaction and isomerization reaction, respectively. The main consumption path of C_3H_7 is its β-C−C dissociation reaction to generate C_2H_4 and methyl radicals. C_3H_6 is mainly generated by the 1-$C_3H_7NO_2$ CME reaction, and its consumption is by reaction with H radicals to generate C_2H_4 and methyl groups. Simultaneously, C_2H_4 is mainly consumed via the hydrogen abstraction reaction by H and OH to produce C_2H_3, which is further decomposed into C_2H_2.

Although NO_2 also has multiple generation channels, due to the high reactivity under the experimental conditions, the experimental and simulation results show that the NO_2 concentration is relatively lower than other intermediates in the pyrolysis of 1-$C_3H_7NO_2$. The reduction process of NO_2 to NO is mainly carried out by its reaction with H, and its reaction with C_1 hydrocarbon groups (CH_2 and CH_3) also consumes a small amount of NO_2.[54,54] NO is the main product of HONO decomposition, and HONO also generates OH, which is beneficial to the hydrogen abstraction reaction of hydrocarbon components and 1-$C_3H_7NO_2$. For primary nitromethane decomposition, the main products are CH_3 radicals and NO_2, which easily react with each other to generate NO and CH_3O radical.[54,55] In contrast, similar to nitroethane,[39] the interaction of hydrocarbon radicals with nitrogen oxides is less critical for 1-$C_3H_7NO_2$. This could be due to two reasons. First, the CME channel, one of the initial decomposition pathways of 1-$C_3H_7NO_2$, is strongly competitive, and the generated C_2H_4 and C_3H_6 are less reactive than C_3H_7, while the generated HCNO and HONO do not react directly with hydrocarbon components. Second, the interaction between NO_2 and C_2 and C_3 hydrocarbons is less significant than the interaction between NO_2 and C_1 hydrocarbons.

4.2. Effect of 1-$C_3H_7NO_2$ on the Conversion of n-$C_{10}H_{22}$.

Figures 5 and S1−S5 present the simulated and experimental mole fractions of n-$C_{10}H_{22}$, 1-$C_3H_7NO_2$, and the initiated pyrolysis products at 30 and 760 Torr. The kinetic model developed in this work satisfactorily reproduces the consumption of fuel and the generation of pyrolysis products.

The decomposition of hydrocarbon is a process of decomposing from large to small molecules, and the saturation gradually decreases. According to the mole fractions of species in pure and initiated n-$C_{10}H_{22}$ pyrolysis in our work, under the current experimental conditions, with the increase of temperature, the mole fractions of larger alkenes (C_4−C_{10}) first increased and then decreased. During the pure n-$C_{10}H_{22}$ pyrolysis, the typical profile of larger alkene is a slim peak, while during the initiated pyrolysis, it is a broad peak. The reason for this phenomenon is the addition of an initiator. Take C_5H_{10} as an example, a rate of production analysis (ROP) was carried out, and integrate the rate of formation and consumption along the reactor at different temperatures. The results are shown in Figure 6.

Under a pressure of 760 Torr, the initial formation temperatures of C_5H_{10} in pure and initiated pyrolysis are 870 and 720 K, and the initial consumption temperatures are 975 and 850 K, respectively. The existence of the initiator reduces the formation and consumption temperature of C_5H_{10} and expands the temperature range in which C_5H_{10} exists. Since the initiator is almost completely consumed at 850 K, the formation rate of C_5H_{10} changes relatively flat when the temperature exceeds 850 K. In the temperature range of 850−1000 K, the consumption rate of n-pentane increases slowly, so the change in production rate and consumption rate leads to a slight change in the overall production of C_5H_{10} in this temperature range. The influence of the initiator on the alkene production and consumption process leads to different trends in initiated and pure n-decane pyrolysis.

https://doi.org/10.1021/acsomega.3c00508
ACS Omega 2023, 8, 15384−15396

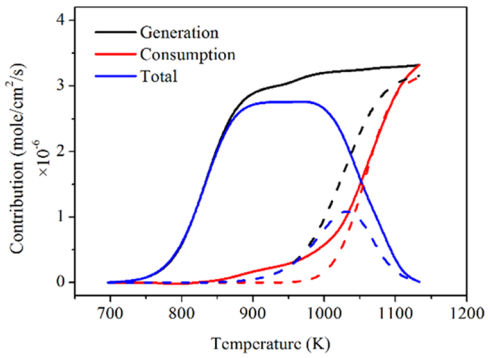

Figure 6. Integrated contributions from reaction during the generation and consumption of C_5H_{10} as a function of temperature at 760 Torr. Solid lines are for initiated n-$C_{10}H_{22}$ pyrolysis, and dashed lines are for pure n-$C_{10}H_{22}$ pyrolysis.

Figure 7 shows the pyrolysis rates of n-$C_{10}H_{22}$ and 1-$C_3H_7NO_2$ in pure and initiated pyrolysis with temperature under different pressures. The interaction between n-$C_{10}H_{22}$ and 1-$C_3H_7NO_2$ affected the initiation temperature of pyrolysis during the initiation of the pyrolysis reaction. As shown in Figure 6, when 1-$C_3H_7NO_2$ exists, the initial decomposition temperature of n-$C_{10}H_{22}$ reduces in varying degrees under different reaction pressure conditions. Under the reaction pressures of 30 and 760 Torr, the addition of 1-$C_3H_7NO_2$ initiator caused the initial pyrolysis temperature of n-$C_{10}H_{22}$ to decrease from 980 and 846 K to 900 and 721 K, respectively. At the same time, compared with the pure n-$C_{10}H_{22}$ pyrolysis, the addition of 1-$C_3H_7NO_2$ improved the pyrolysis rate of n-$C_{10}H_{22}$ at the same temperature. Since the temperature and pressure conditions of n-$C_{10}H_{22}$ pyrolysis and n-$C_{10}H_{22}$/1-$C_3H_7NO_2$-initiated pyrolysis experiments are the same, the promoting effect on n-$C_{10}H_{22}$ pyrolysis is due to the free radicals generated during the pyrolysis process of the added 1-$C_3H_7NO_2$ affect n-$C_{10}H_{22}$ pyrolysis.

Figure 7 also shows that the promoting effect of 1-$C_3H_7NO_2$ on the pyrolysis of n-$C_{10}H_{22}$ increases with increasing pressure, which illustrates that the higher pressure is favorable for the initiator to promote the pyrolysis of hydrocarbon fuel. Based on the free-radical reaction mechanism of hydrocarbon fuel, this phenomenon can be explained by the increase in pressure enhancing the bimolecular reaction process during pyrolysis, especially the reaction of active small free radicals with n-$C_{10}H_{22}$. Contrary to the fact that n-$C_{10}H_{22}$ pyrolysis is promoted under the influence of n-$C_{10}H_{22}$, the pyrolysis of 1-$C_3H_7NO_2$ will be inhibited to a lower degree, mainly due to the small-molecule reactive radicals (such as OH, CH_3, and H) easily reacting with n-$C_{10}H_{22}$, which accelerates the pyrolysis of n-$C_{10}H_{22}$ but also reduces the number of free radicals that can react with 1-$C_3H_7NO_2$, thereby inhibiting the consumption of 1-$C_3H_7NO_2$.

Previous research has shown that initiators can effectively promote the pyrolysis of hydrocarbon fuel and increase the pyrolysis rate, thereby significantly improving the total heat-sink capacity of fuel within a given temperature.[11,20,21] The results in Figure 7 show the promoting effect of the 1-$C_3H_7NO_2$ initiator on n-$C_{10}H_{22}$ pyrolysis, reflecting the overall effect of 1-$C_3H_7NO_2$ on the fuel pyrolysis rate. When the fuel flows through the reactor or the heat exchange channel, the change in the pyrolysis rate along the tube directly affects the endothermic process of the fuel and the heat exchange in the channel. Therefore, to analyze the influence of the initiator on the fuel pyrolysis rate distribution, we defined dc/dL as the conversion rate of n-$C_{10}H_{22}$ along the unit length of the reactor. Since the pyrolysis situation in the flow tube cannot be detected, this paper uses the model to calculate the results of dc/dL. Figure 8 shows the simulated results of T_{max} = 1314 and

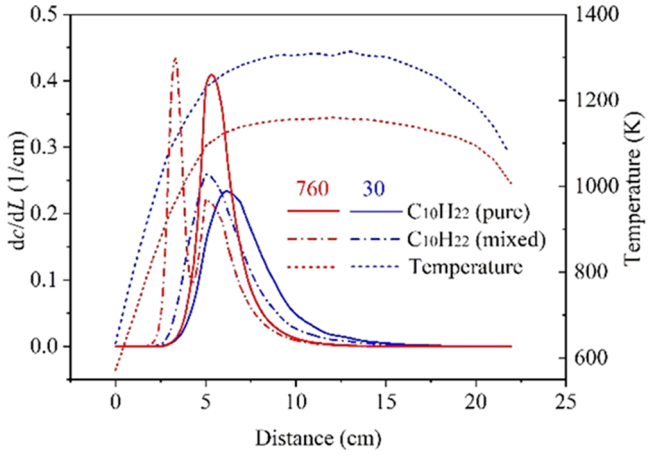

Figure 8. Conversion rate of n-$C_{10}H_{22}$ in pure n-$C_{10}H_{22}$ pyrolysis (solid lines) and initiated pyrolysis (dot dashed lines) at unit length along with the reactor distance at 30 and 760 Torr.

1160 K under 30 and 760 Torr pressure conditions, respectively. It can be seen from Figure 8 that dc/dL of n-$C_{10}H_{22}$ first increased and then decreased and was completely consumed entirely at 15 cm. In the pyrolysis of pure n-$C_{10}H_{22}$, under the selected temperature conditions, the increase in temperature will increase the decomposition rate, thereby promoting the pyrolysis of n-$C_{10}H_{22}$; however, as n-$C_{10}H_{22}$ is consumed in the flow process, although the reaction

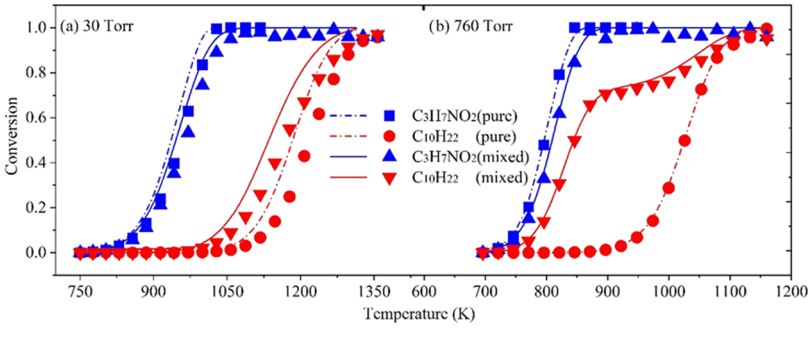

Figure 7. Simulated (solid lines) and experimental (symbols) conversion of n-$C_{10}H_{22}$ and 1-$C_3H_7NO_2$ at 30 and 760 Torr.

https://doi.org/10.1021/acsomega.3c00508
ACS Omega 2023, 8, 15384−15396

temperature still shows an upward trend, the fuel consumption rate is gradually dominated by the concentration as its concentration decreases. The effects of these two aspects cause a peak in dc/dL of the fuel during the flow.

In the process of initiated pyrolysis, under the current temperature and pressure conditions, dc/dL of n-$C_{10}H_{22}$ has different trends under different pressures. Figure 8 also shows that at a pressure of 30 Torr, adding 1-$C_3H_7NO_2$ increases dc/dL of n-$C_{10}H_{22}$ at a lower temperature so that the peak of dc/dL appears at a lower temperature. At 760 Torr, dc/dL of n-$C_{10}H_{22}$ has two peaks, which appear at 3.2 and 5.0 cm. The main reason for the appearance of the previous peak is that the pyrolysis of 1-$C_3H_7NO_2$ promotes the pyrolysis of n-$C_{10}H_{22}$. Figure 9 shows that the consumption of 1-$C_3H_7NO_2$ after 3.2

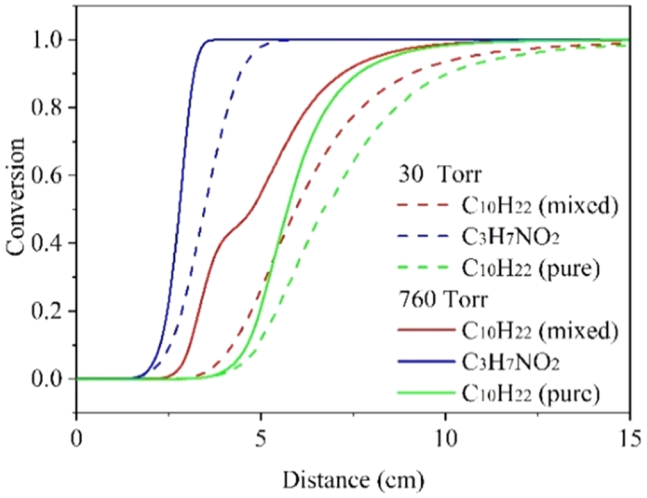

Figure 9. Conversion of n-$C_{10}H_{22}$ and 1-$C_3H_7NO_2$ along with the reactor distance at 30 Torr, 1314 K and 760 Torr, 1160 K.

cm has exceeded 90%, and the promotion effect on the pyrolysis of n-$C_{10}H_{22}$ is negligible, so dc/dL of n-$C_{10}H_{22}$ decreases rapidly. The last peak appears at 5.0 cm, which is caused by the combination of two factors, the increase in temperature and the decrease in concentration. Figure 8 also shows that between 3.2 and 5.0 cm, the variation in the n-$C_{10}H_{22}$ conversion rate showed a trend of first decreasing and then increasing.

To further investigate the effect of 1-$C_3H_7NO_2$ on the reaction kinetics of n-$C_{10}H_{22}$ pyrolysis, ROP analysis of n-$C_{10}H_{22}$ along the flow direction was carried out under the conditions of T_{max} = 1160 K and a pressure of 760 Torr. Due to the symmetrical structure of n-$C_{10}H_{22}$, the C−C bond has five positions where dissociation reactions can occur. The C−C bond dissociation reaction generates n-alkane radicals of C_1−C_9, and the radical attack reaction can generate five kinds of $C_{10}H_{21}$ radicals. To simplify the display of ROP analysis results in the figure, the rate of each type of reaction is the sum of the rates of five reactions in each type.

The results in Figure 10 indicate that n-$C_{10}H_{22}$ is consumed by its C−C bond dissociation reaction and the attack of H, CH_3, and OH small-molecule radicals on n-$C_{10}H_{22}$ to abstract H. During the pure pyrolysis of n-$C_{10}H_{22}$, the C−C bond dissociation reaction is the initial reaction of n-$C_{10}H_{22}$ pyrolysis. In the following pyrolysis process, the reactions of H and CH_3 attacking n-$C_{10}H_{22}$ occur almost simultaneously. Due to the lower reaction activation energy, these reactions

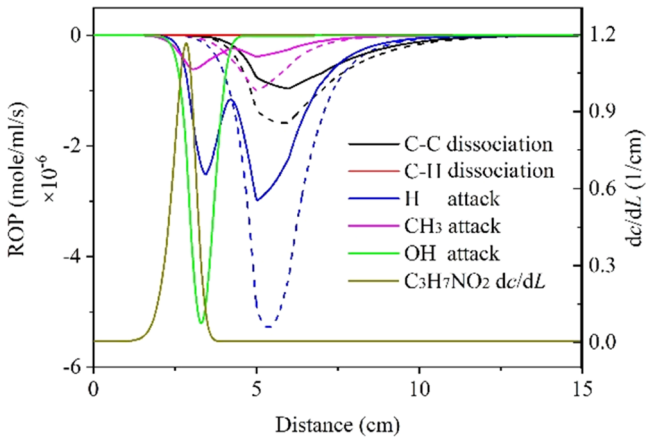

Figure 10. ROP analysis of n-$C_{10}H_{22}$ in pure n-$C_{10}H_{22}$ pyrolysis (dashed lines) and initiated pyrolysis (solid lines) along with the reactor distance at 760 Torr, and T_{max} = 1160 K.

contribute more to fuel consumption than C−C bond dissociation reactions. As shown in Figure 10, in the initiation pyrolysis, 1-$C_3H_7NO_2$ as an initiator will generate CH_3, OH, and H radicals, which react with n-$C_{10}H_{22}$ to make the n-$C_{10}H_{22}$ consumption reactions happen earlier. Among them, whether it is the pure pyrolysis of n-$C_{10}H_{22}$ or the initiated pyrolysis, the hydrogen abstraction reaction of H on the fuel has a high contribution to the consumption of the fuel; in the initiated pyrolysis, the OH radical generated by the pyrolysis of 1-$C_3H_7NO_2$ also contributes to the n-$C_{10}H_{22}$ pyrolysis process. It can be seen from the figure that this type of reaction has the highest contribution before the complete consumption of 1-$C_3H_7NO_2$, and with the consumption of 1-$C_3H_7NO_2$, it shows a trend of first rising and then falling. In the initiated pyrolysis, there are two peaks in the reactions of H and CH_3 attacking n-$C_{10}H_{22}$ to abstract H, and the former peak is caused by the decomposition of 1-$C_3H_7NO_2$. The last peak is caused by the decomposition of n-$C_{10}H_{22}$ to generate small-molecule free radicals after 1-$C_3H_7NO_2$ is consumed completely.

To reveal the influence of each reaction in the model on the pyrolysis of n-$C_{10}H_{22}$, a reaction sensitivity analysis of n-$C_{10}H_{22}$ was carried out under a pressure of 760 Torr and T_{max} = 1160 K. In the pure pyrolysis of n-$C_{10}H_{22}$, because the initial reaction of n-$C_{10}H_{22}$ pyrolysis is its own C−C bond dissociation reaction, this type of reaction has high sensitivity. While the C−H bond dissociation reaction with a higher energy barrier is difficult to occur, the contribution and sensitivity to n-$C_{10}H_{22}$ are low. The hydrogen abstraction reaction of free radicals is the main pathway of n-$C_{10}H_{22}$ consumption. In the process of n-$C_{10}H_{22}$ pyrolysis, H and CH_3 are mainly involved in this kind of reaction, and the reaction of H attacking fuel to abstract H has high sensitivity. In n-$C_{10}H_{22}$ pyrolysis initiated by 1-$C_3H_7NO_2$, the hydrogen abstraction reaction still has a high sensitivity. However, the sensitivity of the dissociation reaction of the C−C bond of n-$C_{10}H_{22}$ decreases because of the addition of the initiator. The sensitivity of the dissociation reaction increases accordingly as the initiator 1-$C_3H_7NO_2$ is consumed.

As shown in Figure 11, when the n-$C_{10}H_{22}$ pyrolysis rate is below 50%, the 1-$C_3H_7NO_2$ C−N bond dissociation reaction has the highest sensitivity to n-$C_{10}H_{22}$ consumption because the CH_3, H, and OH radicals generated during the 1-$C_3H_7NO_2$ decomposition reaction are conducive to the consumption of

https://doi.org/10.1021/acsomega.3c00508
ACS Omega 2023, 8, 15384−15396

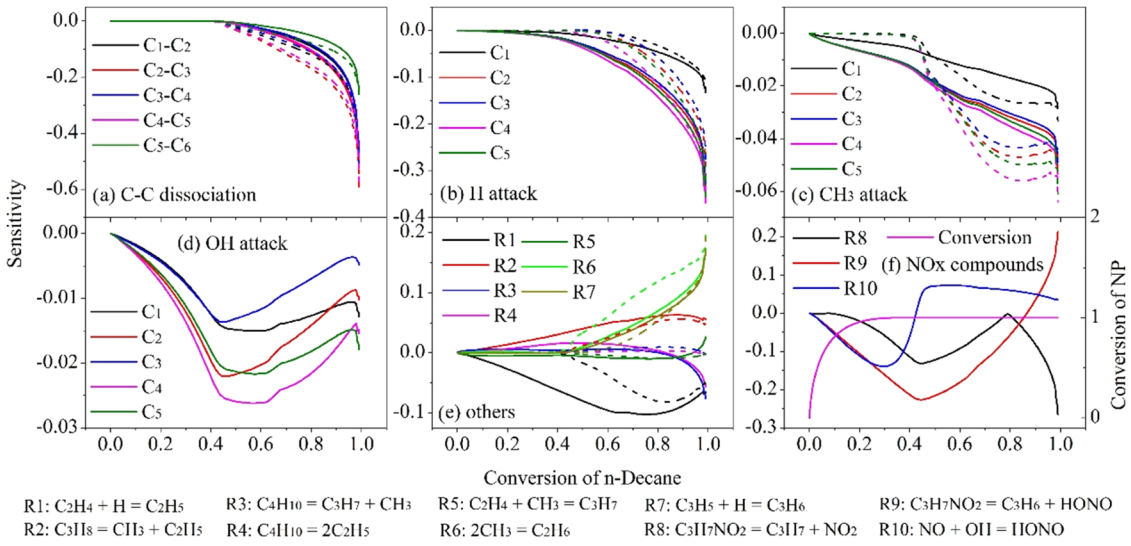

Figure 11. Sensitivity analysis of n-$C_{10}H_{22}$ in pure n-$C_{10}H_{22}$ pyrolysis (dashed lines) and initiated pyrolysis (solid lines) corresponding to T_{max} = 1160 K at 760 Torr.

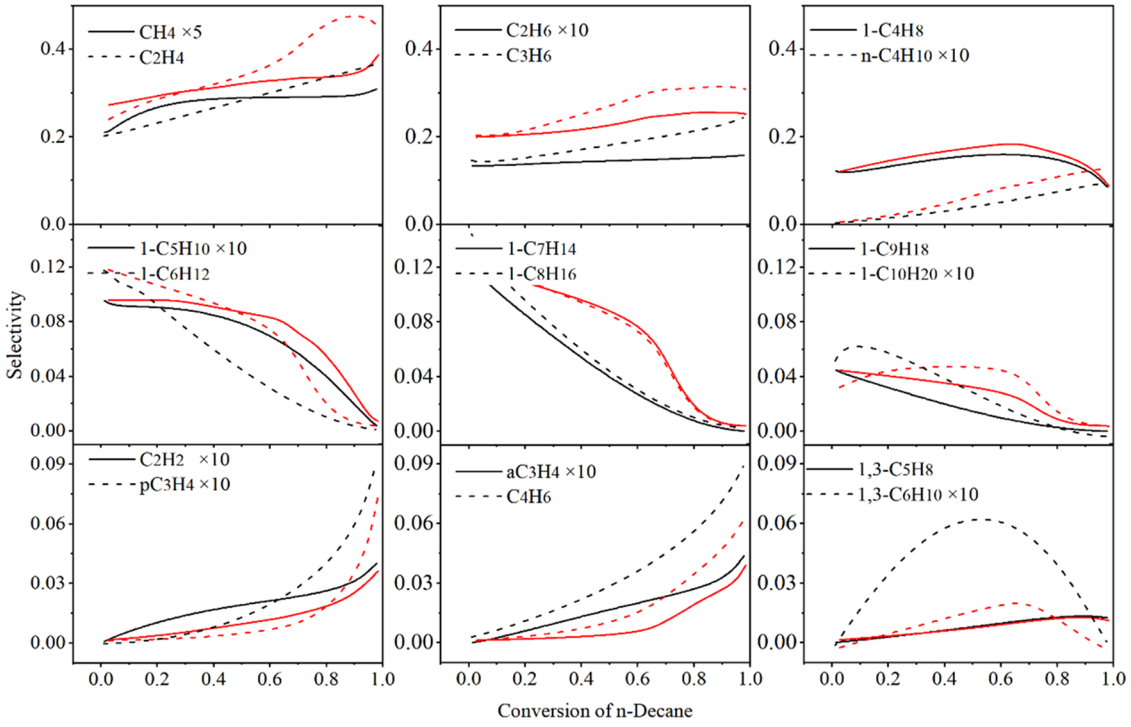

Figure 12. Selectivity of major pyrolysis products in pure n-$C_{10}H_{22}$ pyrolysis (black) and initiated n-$C_{10}H_{22}$ pyrolysis (red) at 760 Torr.

n-$C_{10}H_{22}$. As shown in Figure 11f, when the n-$C_{10}H_{22}$ pyrolysis rate is above 50%, its contribution to n-$C_{10}H_{22}$ consumption gradually decreases because the generation of reactive radicals from the pyrolysis of 1-$C_3H_7NO_2$ gradually decreases with the consumption of 1-$C_3H_7NO_2$, eventually approaching zero. In addition, other reactions that consume more or generate free radicals, such as H or CH_3, are also highly sensitive to the consumption of n-$C_{10}H_{22}$. As shown in Figure 11e, reaction R1 easily cracks to generate H and is conducive to the consumption of n-$C_{10}H_{22}$; reactions R2, R6, and R7 consume small-molecule free radicals, which is not conducive to the pyrolysis of n-$C_{10}H_{22}$.

4.3. Effect of 1-$C_3H_7NO_2$ on the Distribution of n-$C_{10}H_{22}$ Pyrolysis Species. The addition of 1-$C_3H_7NO_2$ also has a specific effect on the distribution of pyrolysis products under the experimental conditions in this work. Figure 12 compares the selectivity of the main products of n-$C_{10}H_{22}$ pure pyrolysis and initiated pyrolysis, mainly including alkanes (methane and ethane), 1-alkenes (1-alkenes of C_2−C_{10}), diolefins (1,3-C_6H_{10}, C_4H_6, 1,3-C_5H_8, and aC_3H_4), and alkynes (pC_3H_4 and C_2H_2). The product selectivity is defined as the ratio of the total mole fraction of C atoms of the components to the total C atoms mole fraction of n-$C_{10}H_{22}$ consumed.

Compared with the pure pyrolysis of n-$C_{10}H_{22}$, the initiated pyrolysis significantly increased the generation of CH_4 and C_2H_4, C_2H_6, and C_3H_6. According to the ROP analysis, CH_4 was mainly generated by CH_3 attacking n-$C_{10}H_{22}$ to abstract H, and more than 90% of C_2H_6 was generated by the

https://doi.org/10.1021/acsomega.3c00508
ACS Omega 2023, 8, 15384−15396

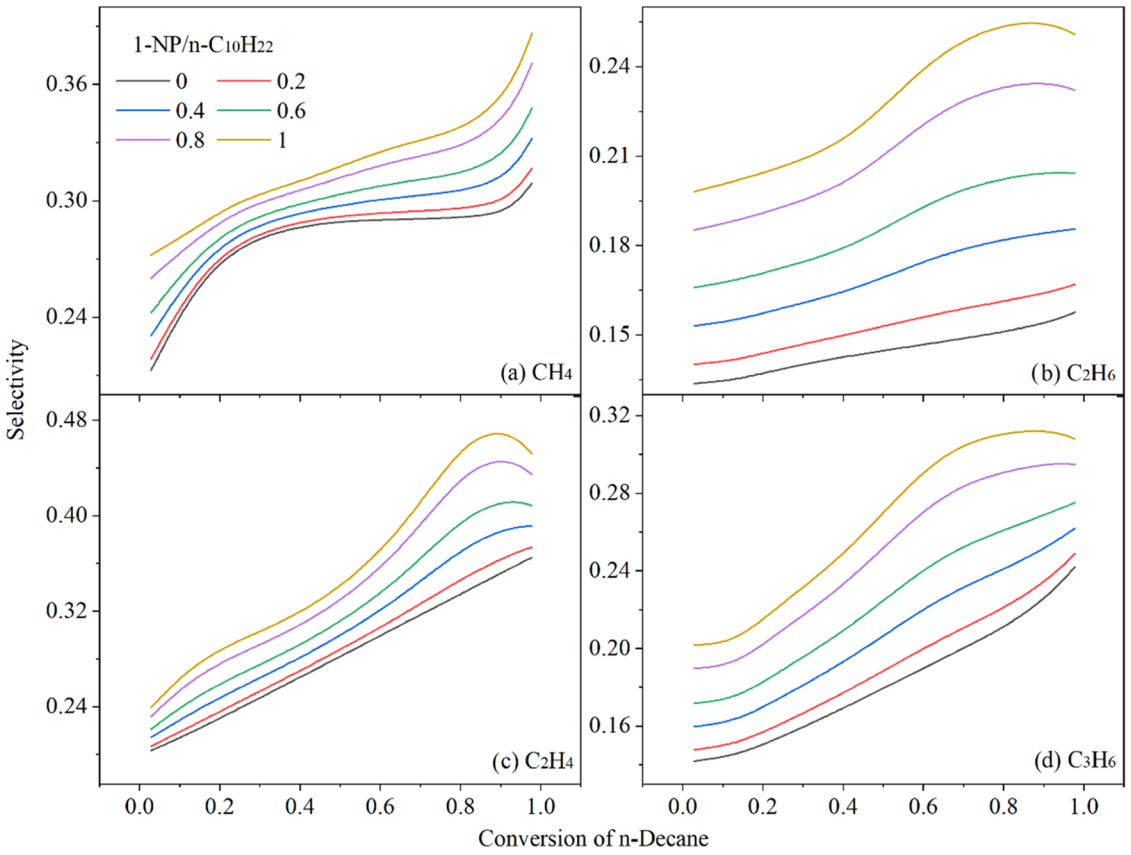

Figure 13. Influence of 1-$C_3H_7NO_2$ concentration on the selectivity of initiated pyrolysis species of *n*-$C_{10}H_{22}$, (a) CH_4, (b) C_2H_6, (c) C_2H_4, and (d) C_3H_6.

recombination of CH_3. Although the initial pyrolysis of 1-$C_3H_7NO_2$ does not produce CH_3, the main consumption path of C_3H_7 generated by the dissociation of its C−N bond is $C_3H_7 = C_2H_4 + CH_3$, and the contribution rate is ∼80%. Therefore, the addition of 1-$C_3H_7NO_2$ can increase the generation of CH_3, and then CH_3 promotes the production of CH_4 and C_2H_6. At the same time, C_2H_4 and C_3H_6 are the products of the CME pathway of the initial pyrolysis pathway of 1-$C_3H_7NO_2$, which will inevitably lead to the improvement of the selectivity of these two components.

As shown in Figure 12, the addition of 1-$C_3H_7NO_2$ slightly increases the selectivity of C_3−C_9 olefins but dramatically reduces the selectivity of diolefins (1,3-C_6H_{10},1,3-C_5H_8, C_4H_6, and aC_3H_4) and alkynes (pC_3H_4 and C_2H_2). To analyze the reasons for this phenomenon, the most significant conditions for 1-$C_3H_7NO_2$ to promote the pyrolysis of n-$C_{10}H_{22}$ were selected for analysis. At this time, the pyrolysis rate of *n*-$C_{10}H_{22}$ was 15%, and the temperature was 954 K. When the pure pyrolysis of *n*-$C_{10}H_{22}$ reached 15%, the temperature was 1083 K. ROP analysis was performed on typical olefins such as 1-butene and propylene. These two alkenes are mainly generated through *β*-C−C dissociation of the C_6H_{13} radical, which decomposes into dienes or alkynes. Taking 1-butene as an example, in the pure pyrolysis process of n-$C_{10}H_{22}$, its decomposition proceeds through hydrogen abstraction reactions (R1−R4), and the products are two C_4H_7 radicals, C_3H_6 and C_2H_4, and C_4H_7 will continue to crack to generate C_4H_6. The ratio of the contribution of these four reactions is 1:1:2:0.6

$$C_4H_8 - 1 + H = H_2 + C_4H_7 - 1 \quad (R1)$$

$$C_4H_8 - 1 + H = H_2 + C_4H_7 - 2 \quad (R2)$$

$$C_4H_8 - 1 + H = CH_3 + C_3H_6 \quad (R3)$$

$$C_4H_8 - 1 + H = C_2H_5 + C_2H_4 \quad (R4)$$

When the initiator 1-$C_3H_7NO_2$ is added, the OH generated during the pyrolysis process will also abstract the H on 1-butene to generate H_2O and C_4H_7 radicals (R5 and R6). The contribution of each reaction to the consumption of C_4H_8-1 is ∼15%

$$C_4H_8 - 1 + OH = H_2O + C_4H_7 - 1 \quad (R5)$$

$$C_4H_8 - 1 + OH = H_2O + C_4H_7 - 2 \quad (R6)$$

During the pure pyrolysis of n-$C_{10}H_{22}$, as shown in reactions R7 and R9, C_3H_6 reacts with H and CH_3 radicals to generate aC_3H_5 radicals and C_2H_4, and the three reactions contributed 28, 35, and 37% to the consumption of C_3H_6, respectively. In the initiated pyrolysis of *n*-$C_{10}H_{22}$/1-$C_3H_7NO_2$, in addition to the above three reactions, C_3H_6 will also react with OH radicals to form aC_3H_5 (as shown in reaction R10). The four reactions contributed 25, 30, 29, and 16% to C_3H_6 consumption. Furthermore, the decomposition paths of aC_3H_5 and C_2H_4 are the same as those of *n*-$C_{10}H_{22}$ pyrolysis, $aC_3H_5 \rightarrow aC_3H4 \rightarrow pC_3H_4 \rightarrow C_2H_2$, and $C_2H_4 \rightarrow C_2H_3 \rightarrow C_2H_2$, respectively

$$C_3H_6 + H = H_2 + aC_3H_5 \quad (R7)$$

$$C_3H_6 + H = CH_3 + C_2H_4 \quad (R8)$$

$$C_3H_6 + CH_3 = CH_4 + aC_3H_5 \quad (R9)$$

https://doi.org/10.1021/acsomega.3c00508
ACS Omega 2023, 8, 15384−15396

$$C_3H_6 + OH = H_2O + aC_3H_5 \quad (R10)$$

It can be seen from the above analysis that the pyrolysis of 1-$C_3H_7NO_2$ will generate H, OH, and CH_3 small-molecule active radicals, which will participate in the process of alkene consumption. However, Figure 12 shows that because of the addition of 1-$C_3H_7NO_2$, the generation of diolefins and alkynes is inhibited. Since the addition of an initiator will reduce the pyrolysis temperature of n-$C_{10}H_{22}$, compared with pure pyrolysis, initiated pyrolysis will make the fuel reach the same pyrolysis rate at a lower temperature, and temperature is the main factor affecting the reaction rate of olefin consumption. Therefore, decreasing the reaction temperature reduces the consumption rate of C_3−C_9 olefin, resulting in an increase in the selectivity of these products, as well as a decrease in the formation of diolefins (1,3-C_6H_{10}, C_4H_6, 1,3-C_5H_8, and aC_3H_4) and alkynes (pC_3H_4 and C_2H_2), while also making the production of benzene a vital precursor and intermediate of (PAH) polycyclic aromatic hydrocarbons and carbon deposits reduced.

In order to study the effect of initiator concentration on the selectivity of n-$C_{10}H_{22}$-initiated pyrolysis species, the kinetic model was used to simulate the initiated pyrolysis under different 1-$C_3H_7NO_2$/n-$C_{10}H_{22}$ mole fraction ratios (ranging from 0 to 1). Because the influence of the initiator on CH_4, C_2H_6, C_2H_4, and C_3H_6 is more outstanding than on other species, the influence of the initiator concentration on these four species was analyzed and is shown in Figure 13. The results showed that the selectivity of the four components increased with the increase of the initiator concentration. The initial reaction and supplied free radicals during the decomposition of the initiator are responsible for the enhanced selectivity of these four components. The change of the initiator concentration directly affects the speed of related reactions and the concentration of free radicals, thus affecting the formation of these species, and is positively correlated with the initiator concentration.

5. CONCLUSIONS

The pyrolysis of 1-$C_3H_7NO_2$ and the pyrolysis of n-$C_{10}H_{22}$ initiated by 1-$C_3H_7NO_2$ were studied by using the synchrotron radiation flow-tube pyrolysis experimental device under pressures of 30 and 760 Torr to analyze the initiation mechanism of 1-$C_3H_7NO_2$ on the decomposition of n-$C_{10}H_{22}$. In the experiments, the pyrolysis species were detected and analyzed, a detailed reaction kinetic model including 1769 reactions and 278 species was established, and the initiated pyrolysis of the mixture was simulated, which well reflected the formation and consumption of stable components and important intermediates.

The results showed that the addition of 1-$C_3H_7NO_2$ significantly reduces the initial pyrolysis temperature of n-$C_{10}H_{22}$, and the higher the reaction pressure, the stronger the effect of 1-$C_3H_7NO_2$ on the consumption of n-$C_{10}H_{22}$. During the process of fuel pyrolysis and initiated pyrolysis, the conversion rate increased first and then decreased along the flow reactor, so the conversion rate had a peak, and the addition of the initiator made the peak appear at a lower temperature. Initiated pyrolysis has a higher conversion rate of fuel at lower temperatures than pure pyrolysis and a lower conversion rate of fuel at higher temperatures.

The CH_3, H, and OH radicals generated in the pyrolysis process of 1-$C_3H_7NO_2$ attacked n-$C_{10}H_{22}$ to abstract H, which promoted the progress of the n-$C_{10}H_{22}$ pyrolysis chain reaction and replaced the C−C bond dissociation reaction of n-$C_{10}H_{22}$ as the initial reaction of n-$C_{10}H_{22}$ pyrolysis. The CH_3 generated by the pyrolysis of 1-$C_3H_7NO_2$ increases the production of CH_4 and C_2H_6. The initial decomposition of 1-$C_3H_7NO_2$ can generate C_2H_4 and C_3H_6, which increases the selectivity of these two components. Compared with pure pyrolysis, initiated pyrolysis could achieve the same decomposition rate at lower temperature, thereby reducing the production of unsaturated hydrocarbons (diolefins, alkynes, and benzene) that need to be generated at higher temperatures.

■ ASSOCIATED CONTENT

Supporting Information

The Supporting Information is available free of charge at https://pubs.acs.org/doi/10.1021/acsomega.3c00508.

Experimental and modeling mole fraction profiles of pure n-decane pyrolysis (Figures S1−S3) and n-decane/1-nitropropane-initiated pyrolysis (Figures S4 and S5); temperature distribution in the reactor under 30 Torr (Table S1) and 760 Torr (Table S2) (PDF)

■ AUTHOR INFORMATION

Corresponding Author

Weixing Zhou − *School of Energy Science and Engineering, Harbin Institute of Technology, Harbin 150001 Heilongjiang, P. R. China; Zhengzhou Research Institute of Harbin Institute of Technology, Zhengzhou 450001 Henan, P. R. China;* orcid.org/0000-0002-4138-7657; Email: zhouweixing@hit.edu.cn

Authors

Zhenjian Jia − *School of Energy Science and Engineering, Harbin Institute of Technology, Harbin 150001 Heilongjiang, P. R. China; Zhengzhou Research Institute of Harbin Institute of Technology, Zhengzhou 450001 Henan, P. R. China;* orcid.org/0000-0001-6385-7202

Jiuzhong Yang − *National Synchrotron Radiation Laboratory, University of Science and Technology of China, Hefei 230029 Anhui, P. R. China;* orcid.org/0000-0002-7076-3412

Kaiping Yu − *School of Astronautics, Harbin Institute of Technology, Harbin 150001 Heilongjiang, P. R. China*

Complete contact information is available at: https://pubs.acs.org/10.1021/acsomega.3c00508

Notes

The authors declare no competing financial interest.

■ ACKNOWLEDGMENTS

This research was supported by the Natural Science Foundation of China (52106137).

■ REFERENCES

(1) Huang, W.; Li, L. Q.; Yan, L.; Liao, L. Numerical exploration of mixing and combustion in a dual-mode combustor with backward-facing steps. *Acta Astronaut.* **2016**, *127*, 572−578.

(2) Huang, W.; Li, M. H.; Yan, L. Mixing augmentation mechanism induced by the pseudo shock wave in transverse gaseous injection flow fields. *Int. J. Hydrogen Energy* **2016**, *41*, 10961−10968.

(3) Edwards, T. Liquid fuels and propellants for aerospace propulsion: 1903-2003. *J. Propul. Power* **2003**, *19*, 1089−1107.

(4) Ervin, J. S.; Ward, T. A.; Williams, T. F.; Bento, J. Surface deposition within treated and untreated stainless steel tubes resulting from thermal-oxidative and pyrolytic degradation of jet fuel. *Energy Fuels* **2003**, *17*, 577−586.
(5) Yue, L.; Wu, J.; Gong, Y.; Hou, J.; Xiong, L.; Xiao, C.; Fang, W. Heat transfer and cracking performance of endothermic hydrocarbon fuel when it cools a high temperature channel. *Fuel Process. Technol.* **2016**, *149*, 112−120.
(6) Qin, J.; Zhang, S.; Bao, W.; Zhou, W.; Yu, D. Thermal management method of fuel in advanced aeroengines. *Energy* **2013**, *49*, 459−468.
(7) He, H.; Spadaccini, L.; Sobel, D. In *Endothermic Heat-Sink of Jet Fuels for Scramjet Cooling*, Proceedings of the AIAA/ASME/SAE/ASEE Joint Propulsion Conference & Exhibit, 2002.
(8) Edwards, T.; Calderon, L.; Xiong, Y.; et al. Cracking and depositipon behavior of supercritical hydrocarbon aviation fuels. *Combust. Sci. Technol.* **2006**, *178*, 307−334.
(9) Dewitt, M. J.; Edwards, T.; Shafer, L.; Brooks, D.; Striebich, R.; Bagley, S. P.; Wornat, M. J. Effect of aviation fuel type on pyrolytic reactivity and deposition propensity undersupercritical conditions. *Ind. Eng. Chem. Res.* **2011**, *50*, 10434−10451.
(10) Watanabe, M.; Tsukagoshi, M.; Hirakoso, H.; Adschiri, T.; Arai, K. Kinetics and product distribution of n-hexadecane pyrolysis. *AIChE J.* **2000**, *46*, 843−856.
(11) Wickham, D. T.; Engel, J.; Hitch, B.; Karpuk, M. Initiators for endothermic fuels. *J. Propul. Power* **2001**, *17*, 1253−1257.
(12) Chang, J.; Fan, L.; Fujimoto, K. Enhancement effect of free radical initiator on hydro-thermal cracking of heavy oil and model compound. *Energy Fuels* **1999**, *13*, 1107−1108.
(13) Chang, J.; Fu, Y.; Shibata, Y.; Yoshimoto, M.; Fujimoto, K.; Tsubaki, N. Promotional effect of oxidation pretreatment on hydro-thermal cracking of Canadian oil sand bitumen. *Fuel* **2005**, *84*, 1661−1663.
(14) Chang, J.; Tsubaki, N.; Fujimoto, K. Elemental sulfur as an effective promoter for the catalytic hydrocracking of Arabian vacuum residue. *Fuel* **2001**, *80*, 1639−1643.
(15) Wang, Z.; Guo, Y.; Lin, R. Effect of Triethylamine on the Cracking of Heptane Under a Supercritical Ccondition and the Kinetic Study on the Cracking of Heptane. *Energy Convers. Manage.* **2008**, *49*, 2095−2099.
(16) Wang, Z.; Guo, Y.; Lin, R. Pyrolysis of Hydrocarbon Fuel ZH-100 Under Different Pressures. *J. Anal. Appl. Pyrolysis* **2009**, *85*, 534−538.
(17) Wang, Z.; Lin, R. Theoretical study on the reaction route for the major liquid product from pyrolysis of triethylamine. *J. Anal. Appl. Pyrolysis* **2008**, *81*, 205−210.
(18) Wang, Z.; Lin, R.; Fang, W.; Li, G.; Guo, Y.; Qin, Z. Triethylamine as an initiator for cracking of heptane. *Energy* **2006**, *31*, 2773−2790.
(19) Priyadarshi, S.; Kishore, M. S. N.; Vinu, R. Analytical pyrolysis of jet fuel using different free radical initiators to produce low molecular weight hydrocarbons. *J. Anal. Appl. Pyrolysis* **2022**, *162*, 105430.
(20) Wickham, D. T.; Engel, J.; Rooney, S.; Hitch, B. D. Additives to increase fuel heat sink capacity in a fuel/air heat exchanger. *AIAA J.* **2005**, *3*, 916.
(21) Wickham, D. T.; Engel, J. R.; Rooney, S.; Hitch, B. D. Additives to improve fuel heat sink capacity in air/fuel heat exchangers. *J. Propul. Power* **2008**, *24*, 55−63.
(22) Liu, G.; Han, Y.; Guo, W.; Zhang, X.; Wang, L.; Mi, Z. Supercritical initiative cracking of endothermic fuel model compound n-dodecane with 1-nitropropane. *AIAA J.* **2008**, *5*, 127.
(23) Liu, G.; Han, Y.; Wang, L.; Zhang, X.; Mi, Z. Supercritical thermal cracking of N-dodecane in presence of several initiative additives: Products distribution and kinetics. *Energy Fuels* **2008**, *22*, 3960−3969.
(24) Chakraborty, J. P.; Kunzru, D. High-pressure pyrolysis of n-heptane: Effect of initiators. *J. Anal. Appl. Pyrolysis* **2012**, *95*, 48−55.
(25) Wang, Q.-D.; Hua, X.-X.; Cheng, X.-M.; Li, J.-Q.; Li, X.-Y. Effects of fuel additives on the thermal cracking of n-Decane from reactive molecular dynamics. *J. Phys. Chem. A* **2012**, *116*, 3794−3801.
(26) Guan, Y.; Yang, B.; Qi, S.; Yi, C. Kinetic modeling of the free-radical process during the initiated thermal cracking of normal alkanes with 1-nitropropane as an Initiator. *Ind. Eng. Chem. Res.* **2011**, *50*, 9054−9062.
(27) Guan, Y.; Zhang, Y.; Yi, C.; Yang, B. Understanding the initial decomposition pathways of the n-alkane/nitroalkane binary mixture. *Chin. J. Chem.* **2013**, *31*, 1087−1094.
(28) Qi, F. Combustion chemistry probed by synchrotron VUV photoionization mass spectrometry. *Proc. Combust. Inst.* **2013**, *34*, 33−63.
(29) Jia, Z. J.; Wang, Z. D.; Cheng, Z. J.; Zhou, W. X. Experimental and modeling study on pyrolysis of n-decane initiated by nitromethane. *Combust. Flame* **2016**, *165*, 246−258.
(30) Ward, T. A.; Ervin, J. S.; Zabarnick, S.; Shafer, L. Pressure Effects on Flowing Mildly-Cracked n-Decane. *J. Propul. Power* **2005**, *21*, 344−355.
(31) Westbrook, C. K.; Pitz, W. J.; Herbinet, O.; Curran, H. J.; Silke, E. J. A Comprehensive Detailed Chemical Kinetic Reaction Mechanism for Combustion of n-Alkane Hydrocarbons from n-Octane to n-Hexadecane. *Combust. Flame* **2009**, *156*, 181−199.
(32) Malewicki, T.; Brezinsky, K. Experimental and Modeling Study on The Pyrolysis and Oxidation of n-Decane and n-Dodecane. *Proc. Combust. Inst.* **2013**, *34*, 361−368.
(33) Zeng, M.; Yuan, W.; Wang, Y.; Zhou, W.; Zhang, L.; Qi, F.; Li, Y. Experimental and Kinetic Modeling Study on Oxidation of n-Decane. *Combust. Flame* **2014**, *161*, 1701−1715.
(34) Jia, Z.; Huang, H.; Zhou, W.; Fei, Q.; Zeng, M. Experimental and modeling investigation of n-Decane pyrolysis at supercritical pressures. *Energy Fuels* **2014**, *28*, 6019−6028.
(35) Si, J.; Li, S.; Hang, P.; Ming, D.; Yan, S. Investigation of pressure effect on thermal cracking of n-Decane at supercritical pressures. *Energy Fuels* **2018**, *32*, 4040−4048.
(36) Liu, B.; Zhu, Y.; Yan, J. J.; Lei, Y.; Zhang, B.; Jiang, P. X. Experimental investigation of convection heat transfer of n-decane at supercritical pressures in small vertical tubes. *Int. J. Heat Mass Transfer* **2015**, *91*, 734−746.
(37) Liu, B.; Wang, X.; Zhu, Y. H.; Jiang, P. X. Experimental investigation of convection heat transfer of n-Decane at supercritical pressures in a micro/mini vertical tube. *J. Eng. Thermophys.* **2014**, *35*, 114−118.
(38) Weng, J-J.; Tian, Z-Y.; Zhang, K-W.; Ye, L-L.; Liu, Y-X.; Wu, L-N.; Yu, D.; Yang, J-Z.; Cao, C-C.; Zou, J-B. Experimental and kinetic investigation of pyrolysis and oxidation of nitromethane. *Combust. Flame* **2019**, *203*, 247−254.
(39) Zhang, K.; Glarborg, P.; Zhou, X.; Zhang, L.; Ye, L.; Dayma, G. Experimental and kinetic modeling study of nitroethane pyrolysis at a low pressure: competition reactions in the primary decomposition. *Energy Fuels* **2016**, *30*, 7738−7745.
(40) Wang, Q.; Tang, X.; Yang, J.; Zhai, Y.; Zhang, Y.; Cao, C.; Wang, J. Investigations on Pyrolysis of Isooctane at Low and Atmospheric Pressures. *Energy Fuels* **2019**, *33*, 3518−3528.
(41) Zhang, T.; Wang, J.; Yuan, T.; Hong, X.; Zhang, L.; Qi, F. Pyrolysis of methyl tert-butyl Ether (MTBE). 1. Experimental study with molecular-beam mass spectrometry and tunable synchrotron VUV photoionization. *J. Phys. Chem. A* **2008**, *112*, 10487−10494.
(42) Zhang, T.; Zhang, L.; Hong, X.; Zhang, K.; Qi, F.; Law, C. K.; Ye, T.; Zhao, P.; Chen, Y. An experimental and theoretical study of toluene pyrolysis with tunable synchrotron VUV photoionization and molecular-beam mass spectrometry. *Combust. Flame* **2009**, *156*, 2071−2083.
(43) Zhou, Z.; Du, X.; Yang, J.; Wang, Y.; Li, C.; Wei, S.; Du, L.; Li, Y.; Qi, F.; Wang, Q. The vacuum ultraviolet beamline/endstations at NSRL dedicated to combustion research. *J. Synchrotron Radiat.* **2016**, *23*, 1035−1045.
(44) Zhang, Y.; Cai, J.; Zhao, L.; Yang, J.; Jin, H.; Cheng, Z.; Li, Y.; Zhang, L.; Qi, F. An experimental and kinetic modeling study of three

https://doi.org/10.1021/acsomega.3c00508
ACS Omega 2023, 8, 15384−15396

butene isomers pyrolysis at low pressure. *Combust. Flame* **2012**, *159*, 905−917.
(45) Qi, F.; Yang, R.; Yang, B.; Huang, C.; Wei, L.; Wang, J.; Sheng, L.; Zhang, Y. Isomeric identification of polycyclic aromatic hydrocarbons formed in combustion with tunable vacuum ultraviolet photoionization. *Rev. Sci. Instrum.* **2006**, *77*, 084101.
(46) Li, Y.; Qi, F. Recent applications of synchrotron VUV photoionization mass spectrometry: insight into combustion chemistry. *Acc. Chem. Res.* **2010**, *43*, 68−78.
(47) Cai, J.; Zhang, L.; Zhang, F.; Wang, Z.; Cheng, Z.; Yuan, W.; Qi, F. Experimental and kinetic modeling study of n-butanol pyrolysis and combustion. *Energy Fuels* **2012**, *26*, 5550−5568.
(48) Wang, Z.; Cheng, Z.; Yuan, W.; Cai, J.; Zhang, L.; Zhang, F.; Qi, F.; Wang, J. An experimental and kinetic modeling study of cyclohexane pyrolysis at low pressure. *Combust. Flame* **2012**, *159*, 2243−2253.
(49) He, L.; Li, C.; Shang, Y.; Ning, H.; Shi, J.; Luo, S-N. Ignition characteristics of 1-Nitropropane: Experimental measurements and kinetic modeling. *Fuel* **2022**, *317*, 123385.
(50) Shang, Y.; Shi, J.; Ning, H.; Zhang, R.; Luo, S-N. Significance of reaction CH3 + NO = H2CN + OH in two-stage ignition of nitromethane. *Fuel* **2019**, *256*, 115956.
(51) Wang, R.; Lei, L.; Wang, X-G.; Lu, Y-S.; Song, L.; Ge, H-G.; Shao, X-Z.; Wang, Z-Y.; Zhang, T-L.; Wang, W-L. Theoretical kinetic investigation of thermal decomposition of nitropropane. *Struct. Chem.* **2017**, *28*, 655−666.
(52) Cord, M.; Husson, B.; Lizardo Huerta, J. C.; Herbinet, O.; Glaude, P-A.; Fournet, R.; Sirjean, B.; Battin-Leclerc, F.; Ruiz-Lopez, M.; Wang, Z.; et al. Study of the low temperature oxidation of propane. *J. Phys. Chem. A* **2012**, *116*, 12214−12228.
(53) Wang, H.; Joshi, A. V.; Davis, S. G.; Laskin, A.; Egolfopoulos, F.; Law, C. K.et al. USC Mech Version II. High-Temperature Combustion Reaction Model of H_2/CO/C_1−C_4 Compounds, 2007. http://ignis.usc.edu/USC_Mech_II.htm.
(54) Glarborg, P.; Bendtsen, A. B.; Miller, J. A. Nitromethane dissociation: Implications for the CH3 + NO2 reaction. *Int. J. Chem. Kinet.* **1999**, *31*, 591−602.
(55) Zhang, K.; Li, Y.; Yuan, T.; Cai, J.; Glarborg, P.; Qi, F. An experimental and kinetic modeling study of premixed nitroethane flames at low pressure. *Proc. Combust. Inst.* **2011**, *33*, 407−414.

https://doi.org/10.1021/acsomega.3c00508
ACS Omega 2023, 8, 15384−15396